Light-Harvesting Nanoparticle Core–Shell Clusters with Controllable Optical Output

Dazhi Sun,[†,‡,⊥] Ye Tian,[†,⊥] Yugang Zhang,[†] Zhihua Xu,[†,§] Matthew Y. Sfeir,[†] Mircea Cotlet,[*,†] and Oleg Gang[*,†]

[†]Center for Functional Nanomaterials, Brookhaven National Laboratory, Upton, New York 11973, United States, [‡]Department of Materials Science and Engineering, South University of Science and Technology of China, Shenzhen, Guangdong 518055, China, and [§]Department of Chemical Engineering, University of Minnesota, Duluth, Minnesota 55812, United States. [⊥]D.S. and Y.T. contributed equally to this work.

ABSTRACT We used DNA self-assembly methods to fabricate a series of core–shell gold nanoparticle–DNA–colloidal quantum dot (AuNP–DNA–Qdot) nanoclusters with satellite-like architecture to modulate optical (photoluminescence) response. By varying the intercomponent distance through the DNA linker length designs, we demonstrate precise tuning of the plasmon–exciton interaction and the optical behavior of the nanoclusters from regimes characterized by photoluminescence quenching to photoluminescence enhancement. The combination of detailed X-ray scattering probing with photoluminescence intensity and lifetime studies revealed the relation between the cluster structure and its optical output. Compared to conventional light-harvesting systems like conjugated polymers and multichromophoric dendrimers, the proposed nanoclusters bring enhanced flexibility in controlling the optical behavior toward a desired application, and they can be regarded as controllable optical switches *via* the optically pumped color.

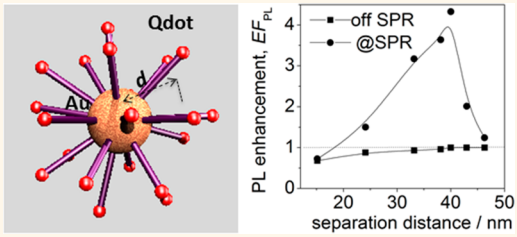

KEYWORDS: nanoparticle · DNA · cluster · quantum dots · fluorescence · self-assembly

Rational design and assembly of colloidal metal and inorganic nanoparticles has stimulated intense research efforts in the past years, especially from the perspective of obtaining nanoclusters with novel optical properties or even with tunable optical response.[1−5] When components like gold nanoparticles and colloidal quantum dots are spaced apart sufficiently so that they do not exchange carriers, the interaction between such nanoparticles is primarily of Coulomb (dipole–dipole) type in the form of energy transfer, specifically photoluminescence quenching by the metal nanoparticle and electromagnetic enhancement, usually seen as an increase in the emitted photoluminescence of the quantum dots.[2−4,6−9] This so-called plasmon–exciton interaction is determined by several factors, including the type, shape, and size of the metal nanoparticles, the electronic properties of the quantum dots, the intercomponent (separation) distance, and the nature of the environment between components.[10−17] Therefore, it is expected that by tuning one or more of such variables in a controlled way one can achieve control and regulation of the optical output from such metal nanoparticle–quantum dot nanostructures.

In this work, we demonstrate the use of DNA-driven assembly methods for the fabrication of nanoclusters with controllable optical outputs. DNA-based approaches are versatile for creating precisely self-assembled organizations of nanoparticles,[18−21] which is advantageous for fabrication of optically active materials.[5,22−27] We propose to assemble core/shell gold nanoparticle (AuNP)–quantum dot (Qdot) nanoclusters with satellite-like architecture, as depicted in Figure 1a, where a large (50 nm size) AuNP functions as the core and several CdSe/ZnS Qdots linked by DNA constitute the shell. DNA was utilized for assembly of both homo- and heteronanoclusters (*e.g.*, like the case of AuNPs and Qdots)[4,13,19,20,28−32] where the distances between nanocomponents could be adjusted by changing the DNA length with single base-pair precision.

* Address correspondence to ogang@bnl.gov, cotlet@bnl.gov.

Received for review December 22, 2014 and accepted May 1, 2015.

Published online May 01, 2015
10.1021/nn507331z

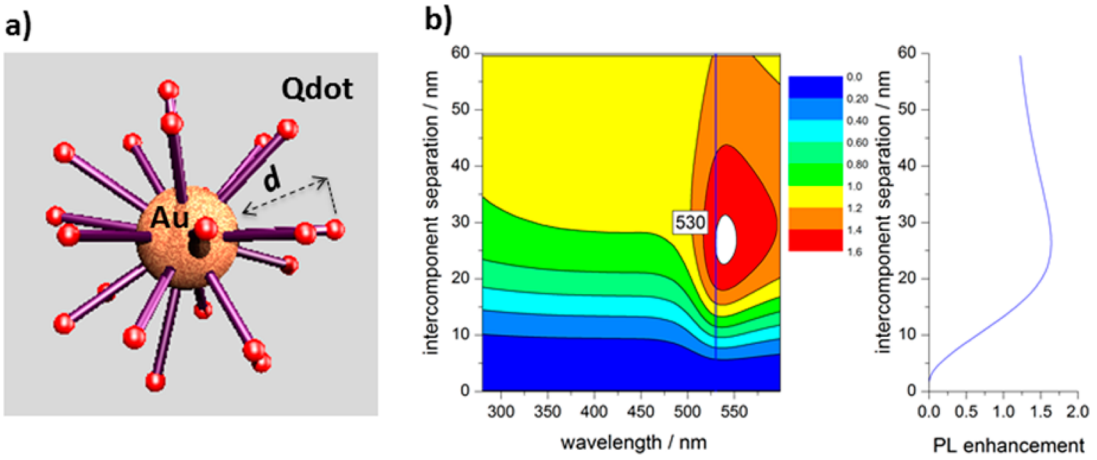

Figure 1. (a) Core−shell AuNP−Qdot nanocluster with satellite-like architecture in which a core AuNP and several CdSe/ZnS Qdots are linked by DNA (purple). (b) Right panel displays the predicted PL enhancement for a coupled AuNP point dipole system as a function of the AuNP−dipole separation distance, *d*, and optical pumping (excitation) wavelength, calculated for a 50 nm size AuNP and a point dipole emitting (in water) at 605 nm. Calculations adapted from refs 11, 33, 34, and 42; see Supporting Information for details. Left panel shows the predicted PL enhancement for optical pumping at the surface plasmon resonance (at 530 nm) as derived from the left panel.

This approach allows for the accurate regulation of interparticle distances with a precision limited by micromechanical properties of DNA constructs. Such architectures mimic the structure of photosynthetic light-harvesting complexes. Apart from the assembly role, the persistence length of hybridized DNA strands, about 50 nm, provides a reasonable structural integrity to assembled nanoclusters in a spatial range relevant for the study of plasmon−exciton interactions. We focus on core−shell nanoclusters incorporating rather large (50 nm sized) AuNPs for two particular reasons. First, such AuNPs can provide electromagnetic enhancement capable of overwhelming the photoluminescence (PL) quenching of Qdots by energy transfer to the metal NP when appropriate intercomponent distances are in place (see below). As such, the proposed nanoclusters can be designed to exhibit plasmon-assisted optical regimes in the form of both enhanced and quenched photoluminescence. Second, a large AuNP core offers a relatively large surface on which several Qdots (here, 20 on average in our assembly) can be connected *via* DNA linkers of similar length on a single AuNP. As such, the proposed core/shell structure represents not only a model system for the investigation of the distance-dependent plasmon−exciton interactions in the case of AuNP and Qdots but also a plasmon-assisted light-harvesting system where Qdots located in the shell harvest the light and transfer it to a "reaction center" represented here by the AuNP core.

The paper is organized as follows: we first describe the proposed design, the self-assembly procedure, and the structural characterization of the AuNP−Qdot core−shell clusters, then demonstrate control (tunability) of the optical signal (PL) for the clusters, from regimes of PL quenching to PL enhancement, by varying the length of the DNA linker connecting the heterocomponents, and finally, we discuss the origin of plasmon-enhanced PL in these cluster architectures.

RESULTS AND DISCUSSION

Nanocluster Design and Its Fabrication *via* Self-Assembly. A metal nanoparticle near a fluorescent molecule and under light illumination can enhance the excitation rate of the molecule by local field enhancement; it can lower the quantum yield by introducing additional nonradiative channels such as energy transfer, in particular, at short metal NP−molecule separation distances, or it can increase the emission rate of the molecule by coupling plasmons and excitons at resonance.[2,11,33] In the assumption that a Qdot can be approximated with a single point dipole, the electromagnetic field distribution for a coupled metal nanoparticle−dipole system can be calculated using the multiple-multipole method.[11,33] Using the method developed by Gersten and Nitzan,[34] we calculated PL enhancement (see Supporting Information) for a coupled AuNP−dipole system in water with the AuNP having 50 nm size and the dipole emitting at 605 nm, as shown in Figure 1b. Such a coupled heterosystem is expected to exhibit PL quenching at separation distances below 13 nm for any given optical pumping wavelength and PL enhancement at separation distances above 13 nm when optically pumped at the surface plasmon resonance (SPR).

Based on the theoretical calculations from Figure 1b, we designed a series of core/shell nanoclusters (NCs) with surface-to-center separation distances (*d*) ranging from ~15 to ~47 nm (Figure 2, left panel, black dots, cluster systems NC1−NC7) between core (AuNP) and shell (Qdot) particles.

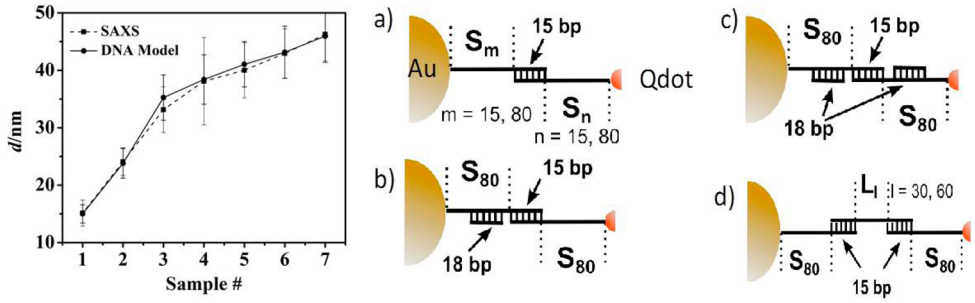

Figure 2. Left: AuNP–Qdot surface-to-center intercomponent distances for a series of AuNP–DNA–Qdot core–shell nanoclusters named herein NC1–NC7, as estimated based on a DNA model (dots and solid line) and synchrotron-based small-angle X-ray scattering measurements (squares and dashed line). Right: DNA linker designs for nanoclusters NC1, NC2, and NC3 (a), NC4 (b), NC5 (c), and NC6 and NC7 (d). See the text for details.

To populate a large range of separation distances for the proposed core/shell nanoclusters, we used three different molecular designs to build the interconnecting DNA linkers. An estimate of AuNP–Qdot surface-to-center separation distance for each case follows after the assembly description. In the first design, for short separation distances (Figure 2a, samples NC1, NC2, and NC3), we utilized a direct hybridization of single-stranded (ss) DNA attached to both AuNPs and Qdots, with ssDNA possessing a 15 base complementary region at the end opposite to the point of attachment to the nanoparticle. The number of unpaired oligonucleotides (S) on the surfaces of AuNPs and Qdots is correspondingly denoted as "*m*" and "*n*". For NC1, we used a 30 base ssDNA connected to each nanoparticle type (Figure 2a, $N_{AuNP} = N_{Qdot} = 30$, $m = n = 15$); for NC2, we used a 95 base ssDNA for AuNPs and a 30 base ssDNA on Qdots (Figure 2a, $N_{AuNP} = 95$, $N_{Qdot} = 30$, $m = 80$, $n = 15$), and for NC3, we used 95 base ssDNA for both types of nanoparticles (Figure 2a, $N_{AuNP} = N_{Qdot} = 95$, $m = n = 80$). As discussed below, the direct hybridization approach provides separation distances of ~15 nm (NC1), ~24 nm (NC2), and ~36 nm (NC3) (Figure 2, left). In the second design, in order to achieve further increase in separation distance, we introduced an additional 18 base-pair dsDNA segment in the linker attached to the AuNP in NC3 (Figure 2a) to obtain NC4 (Figure 2b, $N_{AuNP} = N_{Qdot} = 95$) with a separation distance now increased to about 40 nm (see discussion below). From NC4 to NC5, the separation distance was further increased to 42 nm by the introduction of an additional 15 base-pair dsDNA segment on the Qdot linker, now having three dsDNA segments on the entire linker connecting the AuNP and Qdots (Figure 2c). In the third design, we used a linker-mediated hybridization: AuNPs and Qdots were functionalized with noncomplementary ssDNA strands, each of 95 bases, and nanoparticles were connected by a third ssDNA linker (Figure 2d, L motif), with the linker designed with 15 base complementarity at each end with the strands on the nanoparticles (Figure 2d), and "*l*" represents the number of unpaired single-stranded oligonucleotides in the middle part of linker DNA. For NC6, $l = 30$, and for NC7, $l = 60$. Thus, the separation distances in these cases were 44 and 47 nm, respectively. DNA-functionalized AuNPs and Qdots were mixed in a ratio of 1:20 and aged for 2–3 h before the measurements. Our measurements (Figure S5) indicated that Qdots in the solution were completely consumed due to the reaction and attachment to the AuNP, thus resulting in the formation of clusters in which the AuNP core is surrounded on average by 20 Qdots (see the Supporting Information for the analysis of a cluster population by Monte Carlo simulation). For systems NC4 and NC5, AuNPs and Qdots were each incubated separately with the DNA linker at a 1:10000 molar ratio of nanoparticle/DNA and for about 1 h, and the final solutions were mixed. For systems NC6 and NC7, L_{30} or L_{60} was first incubated with AuNPs for 1 h, and the resulting solution was further mixed with Qdots.

Estimation of Interparticle Distances. First, dynamic light scattering (DLS) was used to measure the size of commercial CdSe/ZnS Qdots covered by a carboxyl-functionalized polymer, before and after functionalization with DNA, and to probe assembled clusters (Figure S4). The polymer-coated Qdot with a 605 nm PL emission peak has a hydrodynamic diameter of ≈10 nm. A Qdot is composed of a CdSe core,[35,36] a ZnS shell, and a carboxyl-functionalized polymer outer shell. We then employed a DNA model reported previously by our group[37,38] to estimate AuNP–Qdot surface-to-center separation distances for the seven cluster systems. In our approach, we used a Daoud-Cotton (DC) blob model to calculate the thickness of tethered DNA on the particle surface and adopted a worm-like chain model to estimate the length of the linker between particles (see Supporting Information for details on calculations). The estimated distances based on the DNA model are plotted in Figure 2, left (dots and solid line), and the derived AuNP–Qdot surface-to-center distances are 15.3 nm (NC1), 24.3 nm (NC2), 36.0 nm (NC3), 39.5 nm (NC4), 41.8 nm (NC5), 44.2 nm (NC6), and 47 nm (NC7).

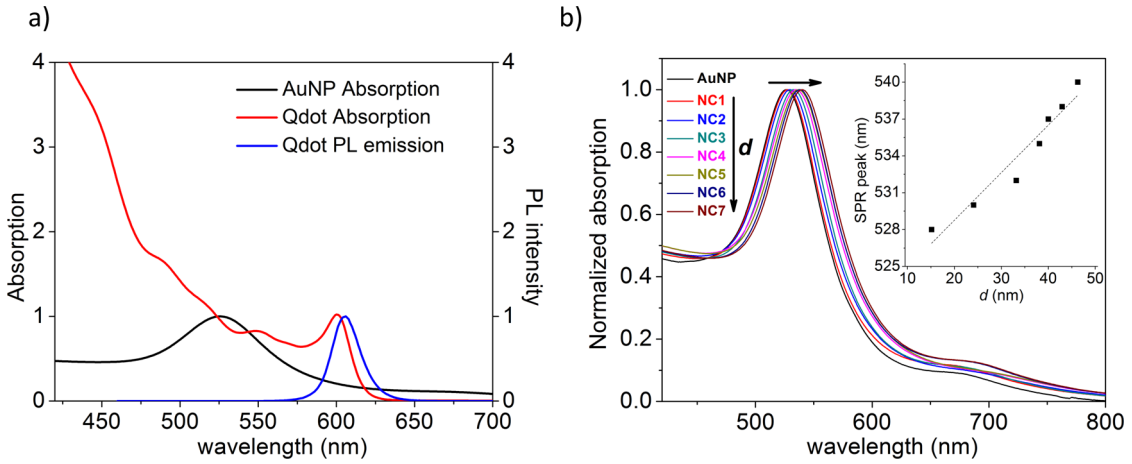

Figure 3. (a) Optical scattering spectrum for 50 nm size AuNPs (black) and UV−vis absorption (red) and photoluminescence (blue) spectra for CdSe/ZnS Qdots in aqueous solution. Scattering and PL spectra are normalized at the peak, while the UV−vis spectrum is normalized at the lowest energy peak. (b) Normalized optical scattering spectra for core/shell AuNP−Qdot nanoclusters with varying DNA linker length. Inset shows the SPR peak *vs* DNA linker length monotonic dependency.

To obtain the detailed information about interparticle separations within clusters, we used synchrotron-based small-angle X-ray scattering (SAXS) measurements at the beamline X9 at the National Synchrotron Light Source (Brookhaven National Laboratory), as shown in Figure 2, left panel (squares and dashed line are derived from data shown in Figure S1, Supporting Information). In order to achieve a sufficient scattering signal, we replaced the Qdots in each of the seven cluster systems with AuNPs of similar diameter (10 nm gold core size), thus obtaining core−shell nanoclusters assembled from gold nanoparticles of two different sizes. These core−shell homonanoclusters of 50 nm AuNP/10 nm AuNP were assembled following an identical recipe as for AuNP−DNA−Qdot nanoclusters, including linker design and assembly procedures, and the corresponding samples are labeled as NC1′−NC7′. Figure S1 illustrates the SAXS patterns measured for samples NC1′−NC7′. By modeling the SAXS data (see Supporting Information), we first obtained the 50 nm Au/10 nm Au surface-to-center distance, and then, after substituting 10 nm Au with a Qdot, we estimated the AuNP−Qdot surface-to-center distance as 15.1 nm (NC1), 24.1 nm (NC2), 33.2 nm (NC3), 38.1 nm (NC4), 40.0 nm (NC5), 42.9 nm (NC6), and 46.3 nm (NC7) (Figure 2 left, squares and dashed line). These values match closely with our calculation based on the DNA model discussed above (Figure 2 left, dots and solid line).

Distance-Dependent Optical Response of Core−Shell Nanoclusters. We show in Figure 3a the spectra of the components making up the core−shell nanoclusters, the optical scattering spectrum of the 50 nm AuNPs (black), as well as the UV−vis absorption (red) and PL (blue) spectra of Qdots. The unique shape of the Qdot's absorption spectrum, increasing toward higher energy, allows selective excitation of the AuNP−Qdot nanocluster outside gold's SPR (for example, here at 440 nm) and at the SPR at 530 nm while monitoring the spectrally narrow PL emitted by the Qdot. This allows probing the distance dependency for both the nonradiative energy transfer from the photoexcited Qdots to the core AuNP and the plasmon-assisted PL enhancement. Accounting for changes in the optical density in the Qdot spectrum from 440 to 530 nm, the overall PL enhancement factor (EF_{PL}) for Qdots in the presence of a AuNP can be calculated using[4]

$$EF_{PL} = \frac{PL(530\,nm)}{PL(440\,nm)} \times \frac{Abs(440\,nm)}{Abs(530\,nm)} \qquad (1)$$

where PL represents the photoluminescence intensity signal measured from the core−shell nanocluster by alternating the optical pumping off and onto the SPR. Figure 3b shows the optical scattering spectra of AuNP−Qdot core−shell nanoclusters of various intercomponent distances, and they feature a monotonic red shift of the SPR peak with increased DNA linker length (Figure 3b, inset). DNA's refractive index (1.76) is higher than that of water (1.33), and an increase in the DNA linker length will result in an increase of the amount of DNA as a dielectric material occupying the space between the AuNP and Qdot components. Therefore, the medium between the components experiences a monotonic increase in the overall dielectric constant with the increase of the DNA linker length. Because the dielectric constant of the medium between the AuNP and Qdot factors in the value of the AuNP's SPR peak, this leads to a monotonic red shift of the SPR peak with increased DNA linker length (Figure 3b).[33] Based on the SPR, we chose the optical pumping with 530 nm: the changes in the scattering profile across the seven core/shell clusters are minimal at this wavelength and so are changes in the scattering cross section (see Figure 3b, inset).

We probed the AuNP−Qdot nanoclusters with time-resolved confocal PL microscopy using alternate pulsed laser excitation at 440 nm/530 nm by employing a time-tagged time-resolved detection mode that

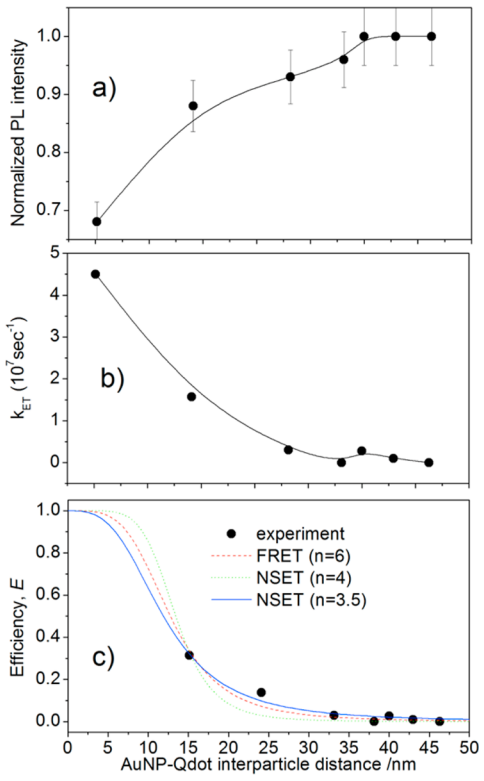

Figure 4. (a) PL intensity *vs* AuNP−Qdot separation distance (dots and black line). Data are normalized to the value corresponding to the longest linker where quenching by a AuNP is negligible. (b) Energy transfer rate (k_{ET}) *vs* AuNP−Qdot separation distance (dots and black line) calculated from PL lifetimes according to eq 2. (c) Energy transfer efficiency (E) *vs* linker length (AuNP−Qdot separation distance) (black dots) with E estimated from PL lifetimes according to eq 4. Fits according to various energy transfer models: nanosurface energy transfer model with $n = 4$ (green dashed line) and $n = 3.5$ (blue solid line) and Förster resonance energy transfer model with $n = 6$ (red dotted line) yielding critical distances of $R_0 = 12.7$, 12.4, and 13.4 nm, respectively.

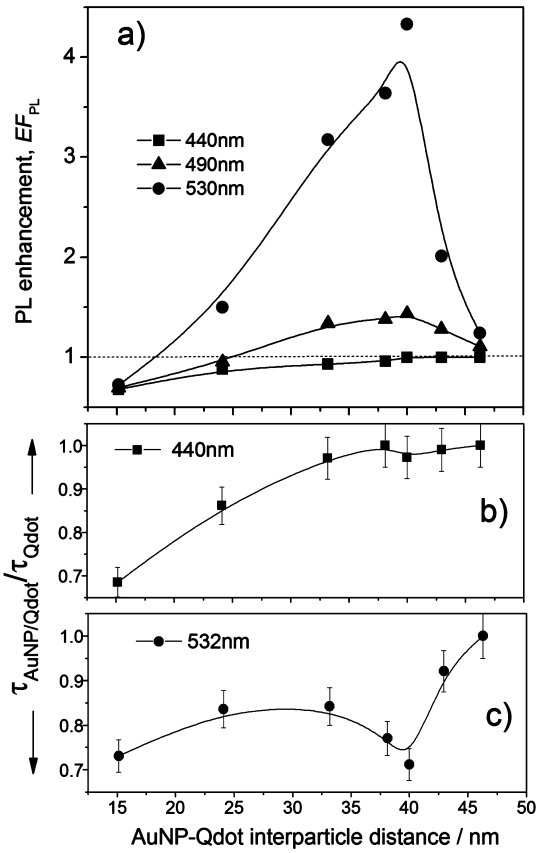

Figure 5. (a) PL enhancement (EF_{PL}) *vs* separation distance (triangle and line) following optical pumping at 440 nm (square and black line), 490 nm (triangle and black line), and 530 nm (dots and black line), with EF_{PL} calculated from PL intensity data according to eq1. (b,c) Normalized PL lifetimes of AuNP−Qdot clusters *vs* separation distance for optical pumping at 440 and 530 nm, respectively. Normalization was done to the PL lifetimes of control samples (Qdots only).

measured simultaneously the PL intensity and PL lifetime from photoexcited nanoclusters freely diffusing in an aqueous solution at low (picomolar) concentration.

Optical Pumping Off-Surface Plasmon Resonance (at 440 nm). Freely diffusing Qdots (control sample) exhibit an average PL lifetime $\tau_{Qdot} = \sim 10.2$ ns. The dependency for the PL intensity and for the energy transfer rate (k_{ET}) *versus* DNA linker length (AuNP−Qdot separation distance) for the seven core−shell nanoclusters following optical pumping off-SPR (440 nm) is shown in Figure 4a,b, respectively. The energy transfer rate was calculated as

$$k_{ET} = 1/\tau_{Qdot/AuNP} - 1/\tau_{Qdot} \quad (2)$$

Here, τ_{Qdot} and $\tau_{Qdot/AuNP}$ are PL lifetimes of Qdots (control sample) and of AuNP−Qdot nanoclusters, respectively, with PL lifetimes estimated as amplitude averaged lifetimes using a biexponential model (see Supporting Information for details). Figure 5b shows the PL lifetime *versus* separation distance for the investigated nanoclusters optically pumped at 440 nm, while Figure S9, contains raw PL decays measured at 440 nm from which PL lifetimes from Figure 5b were extracted.

Both dependencies, in particular, that from Figure 4b, demonstrate separation distance-dependent PL quenching by energy transfer from photoexcited Qdots to AuNPs. The strongest PL quenching (32%) was observed for the shortest DNA linker (~15 nm).

Quenching of fluorescent moieties like colloidal quantum dots and organic fluorescent dyes by proximal metal nanoparticles by energy transfer has been treated analytically by using either a Förster resonance energy transfer (FRET) formalism[13,14,30,39] or a nanosurface energy transfer (NSET) formalism,[30,31,40] or both.[41] Both formalisms are described by a generic formula for the energy transfer efficiency[32]

$$E = \frac{N}{N + (R/R_0)^n} \quad (3)$$

where N is number of metal nanoparticles and R_0 is the critical distance where the efficiency $E = 50\%$. FRET assumes a dipole−dipole coupling mechanism between

the emitting moiety (donor or Qdot) and the metal nanoparticle (acceptor or AuNP) and requires the condition of resonance or spectral overlap between the donor's emission and acceptor's absorption transitions. FRET is a popular formalism for describing dye–dye and Qdot–dye interactions with components separated at distances of 2–10 nm.[42,43] In FRET, donor–acceptor dipole–dipole interaction leads to a $1/R^6$ energy transfer efficiency *versus* distance dependency ($n = 6$, eq 3) with the requirement that donor and acceptor components have strong resonance coupling (spectral overlap) and proper (dipole) orientation. The NSET model considers the emitter as a point dipole transferring to an infinite metal surface, leading to a slower $1/R^4$ distance dependency ($n = 4$ in eq 3) and without a requirement for resonance coupling. FRET has been found to model AuNP emitter systems with short separation distances,[39] while NSET was found to be more suitable for donor–acceptor pairs with larger intercomponent distances.[31,32,40,41] Figure 4c (dots) shows the energy transfer efficiency (E) *versus* separation distance (d) for the seven nanoclusters optically pumped at 440 nm, with the efficiency calculated from the PL lifetimes according to

$$E = 1 - \tau_{\text{Qdot/AuNP}}/\tau_{\text{Qdot}} \quad (4)$$

To model the data from Figure 4c, we consider $N = 1$ in eq 3 and we assume noninteracting adjacent Qdots within a single nanocluster due to the relatively large Qdot–Qdot distance. Indeed, such an assumption is fully justified by our Monte Carlo simulations, which were performed in order to evaluate the surface-to-surface Qdot distances (see Supporting Information and Figure S7), either in the limit of all clusters containing 20 Qdots per AuNP or considering the Poisson distribution of Qdots in shells for the cluster population (Figure S8). We therefore treat the energy transfer interaction in a nanocluster as a single AuNP/Qdot pair. A fit to the data from Figure 4b,c, according to eq 3 where $N = 1$, yields $n = 3.5$ (solid line in Figure 4d), a value which is close to the NSET model ($n = 4$, dashed line in Figure 4d) and far from a FRET model ($n = 6$, dotted line in Figure 4d), and which provides a critical distance $R_{0(\text{NSET})} = 12.4$ nm. Our nanoclusters exhibit large donor–acceptor separation distances and a rather poor spectral overlap (here, the overlap between the Qdot's PL spectrum and the AuNP's SPR band; see Figure 2a), and these conditions favor the NSET model against the FRET model in treating the quenching of Qdot PL by AuNPs by energy transfer. According to the data in Figure 4c,d, energy transfer is extinguished in nanoclusters NC4–NC7, that is, for separation distances around 38 nm and larger. For NSET, the critical distance R_0 is given by[31,32,40]

$$R^4_{0(\text{NSET})} = 0.225 \times \frac{cn^2}{4\pi^2\omega_F k_F} \times \phi_{\text{Qdot}} \times {\lambda_{\text{Qdot}}}^2 \quad (5)$$

being a function of donor quantum yield (ϕ_{Qdot}) and PL emission (λ_{Qdot}), of the Fermi frequency (ω_F) and Fermi vector (k_F) of the acceptor, of the refractive index (n) of the embedding medium, and of the speed of light (c). Using $k_F = 1.2 \times 10^{10}$ m^{-1} and $\omega_F = 8.4 \times 10^{15}$ s^{-1} as values defined for bulk gold,[31] $n = 1.76$ for DNA as the medium filling the space between donor and acceptor, and $\phi_{\text{Qdot}} \approx 0.5$, the NSET critical distance for the energy transfer from Qdots to AuNPs estimated with eq 5 is $R_{0(\text{NSET})} \approx 10.8$ nm, a value close to that obtained from the fit of the data in Figure 4d assuming an NSET model (12.4 nm).

Optical Pumping at Surface Plasmon Resonance (at 530 nm). The PL enhancement (EF_{PL}) *versus* AuNP–Qdot separation distance for the seven nanoclusters subjected to optical pumping at SPR (530 nm) is shown in Figure 5a (dots and line). Also shown in the same graph are the PL enhancements *versus* separation distance estimated from PL intensity data for two other optical pumping wavelengths, off-SPR at 440 nm (square and line) and at 490 nm (triangles and line), an intermediate wavelength. At SPR (at 530 nm), PL enhancement ($\text{EF}_{\text{PL}} > 1$) is observed for nanoclusters with separation distances from around 24 nm and up to 43 nm (NC2–NC6, Figure 2), with the highest value ($\text{EF}_{\text{PL}} = 4.3$) observed for nanocluster NC5 (donor–acceptor separation distance of 40 nm). For the shortest separation distance (NC1, 15 nm), $\text{EF}_{\text{PL}} < 1$, indicating that PL quenching by energy transfer dominates over plasmon-assisted PL enhancement. For the largest separation distance (NC7, 46 nm), $\text{EF}_{\text{PL}} = 1$, which indicates noninteracting Qdots and AuNPs. As such, the designed DNA linkers connecting the donor (Qdot) and acceptor (AuNP) components provide a dynamic range for the plasmon–exciton interaction in our nanoclusters, evolving from regimes of PL quenching to PL enhancement, thus demonstrating the ability to tune the optical output (PL intensity) of a AuNP–Qdot nanocluster by DNA design and DNA self-assembly.

Theoretically, a point dipole emitting at 605 nm and coupled to a 50 nm size AuNP experiences plasmon-assisted PL enhancement for optical pumping at the SPR (at 530 nm) and for separation distances $d > 13$ nm (Figure 1b, left panel, $\text{EF}_{\text{PL}} > 1$), with a maximum EF_{PL} at ~25 nm. Experimentally, we observed $\text{EF}_{\text{PL}} > 1$ for $d =$ ~24 nm and larger and maximal EF_{PL} at $d \sim 40$ nm (Figure 5a, dots and dashed line). These differences between theoretical and experimental data may arise here from the theoretical treatment of the plasmon–exciton interaction with a rather simplistic model[7,11,34,42] in which we assumed that (i) the Qdot is a point dipole with a well-defined transition dipole moment, while recent single-particle studies showed that Qdots do not have a well-defined transition dipole moment;[44] (ii) the nonradiative energy transfer between Qdots and the AuNP is modeled by a FRET formalism, while our

nanoclusters were found experimentally to obey a NSET model (Figure 4d).

Figure 5c shows the changes in PL lifetime with donor−acceptor separation distance for nanoclusters optically pumped at the SPR (at 530 nm). Raw PL decays of nanoclusters following 530 nm optical probing are presented in Figure S9. A clear anticorrelation is seen between the PL enhancement and PL lifetimes vs separation distance (see Figure 5a&5c, dots and line), which could not be observed for optical pumping off-SPR (440 nm) (Figure 5a − 5b, squares and lines). The PL lifetime of a Qdot is $\tau_{Qdot} = 1/(\gamma_r + \gamma_{nr})$, with γ_r and γ_{nr} radiative and nonradiate rates, while the PL quantum yield is $\phi_{Qdot} = \gamma_r/(\gamma_r + \gamma_{nr})$. To understand the origin of the enhancement in both intensity and decay rates occurring at SPR, we can treat the PL emission from a Qdot as a two-step process that involves (i) optical excitation by the incident electrical field which can be perturbed by the local nanoenvironment and (ii) radiation emission; this latter process was determined by the quantum yield of the Qdot.[45] If we assume for simplicity that excitation and emission occur at a similar frequency, $\phi_{Qdot} = \gamma_{em}/\gamma_{exc}$, with γ_{em} being the PL emission rate and γ_{exc} the excitation rate. For a coupled AuNP−Qdot system, the incident light exciting the Qdot will also excite plasmons in the AuNP that can enhance the Qdot's PL quantum yield by increasing the excitation rate, γ_{exc}, and the radiative rate, γ_r. An increase in γ_r requires coupling between the Qdot's exciton and AuNP's plasmon, which is accomplished by a strong spectral overlap between the AuNP's SPR and Qdot's PL emission. In this case, an enhancement in PL intensity is accompanied by an increase in emission rate (decrease in PL lifetime).[10,46] Anticorrelated behavior with PL enhancement accompanied by an increase in the emission rate (decrease in PL lifetime) has been observed previously for isolated terrylene molecules interacting with large 100 nm AuNPs and optically pumped at the SPR,[10] a behavior explained by the fact that the presence of the nearby nanoparticle alters the excitation electric field at the emitter's position, enhancing the excitation rate γ_{exc} and making both the radiative (γ_r) and nonradiative (γ_{nr}) rates strongly distance- and dye- (dipole) orientation-dependent. In that study, the authors acknowledged the importance of the AuNP plasmon resonance in the enhancement process by performing optical pumping away from the resonance to observe a decrease in PL enhancement compared to the condition of the SPR. Similarly, we also observed a reduction in the PL enhancement with the change in optical pumping away from SPR (*e.g.*, from 530 to 490 nm), with the PL enhancement at an optimal separation distance (40 nm, Figure 5a) decreasing from 4.3 (EF_{PL}(530 nm) = 4.3) to 1.44 (EF_{PL}(490 nm) = 1.44), respectively, thus reconfirming the importance of the Au plasmon resonance in enhancing the Qdot's emitted PL. A more recent study[46] reported anticorrelated PL enhancement and PL lifetime *versus* separation distance for CdSe/ZnS Qdots deposited on vertically aligned Au nanorods and optically pumped at the SPR. These authors claimed that the PL enhancement resulted from local enhancement of the excitation electric field due to the presence of the nanostructure which in turn enhanced γ_{exc} (absorption) and γ_r (by Purcell effect).[47] For our AuNP/Qdot nanoclusters, the SPR (530−540 nm) and the Qdot PL spectrum (605 nm) are rather well separated, with little overlap (Figure 3a), which is not expected to promote a strong plasmon−exciton resonant interaction. Consequently, PL enhancement is expected mostly from an increase in γ_{exc}, therefore, we believe this is why changes in PL lifetime from SPR to off-SPR in our case are not as large as those observed in refs 14 (20 times) and 28 (10 times).

CONCLUSIONS

We have shown that by smart design and DNA self-recognition we can create a set of core−shell AuNP−Qdot nanoclusters where the optical output, here photoluminescence, can be controlled by optical pumping color from a quenched to an enhanced state in a stepwise manner. For example, optical excitation off-surface plasmon resonance can produce a quenched PL signal with the quenching rate (efficiency) controlled by the DNA linker length by a $1/d^4$ dependency dictated by nonradiative NSET. For the same set of nanoclusters, optical pumping at the surface plasmon resonance enhances the overall PL, maximally (>4×) for a component separation distance d = 40 nm. An anticorrelation between the PL intensity and PL decay rate was observed for optical pumping at surface plasmon resonance, and this was attributed to an increase in both excitation and radiative rate, leading to enhanced PL intensity and decreased PL lifetime. Compared to conventional light-harvesting systems like conjugated polymers and multichromophoric dendrimers, our nanoclusters bring an enhanced flexibility to control the optical output toward a desired application and can be regarded as controllable optical switches *via* the optically pumped color.

METHODS

AuNPs (50 nm size, Nanopartz Inc.) and carboxyl-functionalized CdSe/ZnS Qdots (Invitrogen, 605 nm PL peak, 10 nm size including polymer coating) were functionalized with thiolated and aminated ssDNA (Integrated DNA Technologies), respectively, and purified according to literature recipes.[29,48] We estimated, on average, about 224 strands of DNA attached per 50 nm AuNP and 10 strands per Qdot (see Supporting Information). Functionalized AuNPs and Qdots dispersed in a

50 mM borate buffer (pH 8.5, 100 mM NaCl) were mixed at a AuNP/Qdot molar ratio of 1:20 in the presence of appropriate ssDNA linker(s) and depending on the particular sample and left to self-assemble onto core/shell nanoclusters by annealing at room temperature for at least 3 h, followed by several washes by centrifugation and finally buffer resuspension, with the supernatant showing no detectable PL signal, thus indicating that all Qdots have bound to AuNPs (Figure S5).

All spectroscopic experiments reported here were performed at room temperature with both Qdots and core−shell nanoclusters in borate buffer (pH 8.5). UV−vis and PL spectra were measured with a PerkinElmer Lambda 25 spectrophotometer and a Varian Cary fluorometer, respectively.

Photoluminescence intensities and lifetimes under laser excitation were measured using an inverted confocal optical microscope equipped with a 1.4 NA, 100× oil immersion objective lens with optical excitation achieved with either a 440 nm or a 530 nm pulsed solid-state laser (LDH440/530, Picoquant, GmbH) using a 10 MHz repetition rate with average power at the sample of 1 μW at 440 nm and 1.2 μW at 530 nm, thus accounting for differences in photon energy for the two colors. The PL emitted by the sample was collected by the same lens, filtered by a dichroic mirror (Semrock 532DRLP), a long-pass filter (Semrock 532 LP), and a 75 μm pinhole before focusing onto a single-photon counting avalanche photodiode connected to a PicoHarp300 time analyzer utilized in time-tagged time-resolved mode. PL intensities and PL lifetimes were estimated with the Symphotime (Picoquant) software. The details of lifetime analysis are given in Supporting Information.

Synchrotron-based SAXS experiments were performed at the National Synchrotron Light Source (NSLS) X-9 beamline, and DLS experiments were performed with a Malvern Zetasizer instrument using a 632 nm He−Ne laser.

Conflict of Interest: The authors declare no competing financial interest.

Acknowledgment. Research was carried out at the Center for Functional Nanomaterials, Brookhaven National Laboratory, which is supported by the U.S. Department of Energy, Office of Basic Energy Sciences, under Contract No. DE-SC0012704. D.S. acknowledges the additional support from National Science Foundation of China (21306077). We thank Dr. A. Chitov for the help with the theoretical model associated with data in Figure 1b.

Supporting Information Available: Determination of the number of ssDNA strands on nanoparticles; determination of AuNP/Qdot assemblies; DNA sequences and sample preparation; DNA modeling for the calculation of interparticle distance; evaluation of the coupling effects between Qdots; time-resolved confocal PL microscopy; and calculation of the theoretical expected PL enhancement. The Supporting Information is available free of charge on the ACS Publications website at DOI: 10.1021/nn507331z.

REFERENCES AND NOTES

1. Giannini, V.; Fernandez-Dominguez, A. I.; Sonnefraud, Y.; Roschuk, T.; Fernandez-Garcia, R.; Maier, S. A. Controlling Light Localization and Light−Matter Interactions with Nanoplasmonics. *Small* **2010**, *6*, 2498–2507.
2. Govorov, A. O.; Bryant, G. W.; Zhang, W.; Skeini, T.; Lee, J.; Kotov, N. A.; Slocik, J. M.; Naik, R. R. Exciton−Plasmon Interaction and Hybrid Excitons in Semiconductor−Metal Nanoparticle Assemblies. *Nano Lett.* **2006**, *6*, 984–994.
3. Zhang, X.; Marocico, C. A.; Lunz, M.; Gerard, V. A.; Gun'ko, Y. K.; Lesnyak, V.; Gaponik, N.; Susha, A. S.; Rogach, A. L.; Bradley, A. L. Experimental and Theoretical Investigation of the Distance Dependence of Localized Surface Plasmon Coupled Forster Resonance Energy Transfer. *ACS Nano* **2014**, *8*, 1273–1283.
4. Maye, M. M.; Gang, O.; Cotlet, M. Photoluminescence Enhancement in CdSe/ZnS-DNA Linked-Au Nanoparticle Heterodimers Probed by Single Molecule Spectroscopy. *Chem. Commun.* **2010**, *46*, 6111–6113.
5. Kuzyk, A.; Schreiber, R.; Zhang, H.; Govorov, A. O.; Liedl, T.; Liu, N. Reconfigurable 3D Plasmonic Metamolecules. *Nat. Mater.* **2014**, *13*, 862–866.
6. Jin, Y. D.; Gao, X. H. Plasmonic Fluorescent Quantum Dots. *Nat. Nanotechnol.* **2009**, *4*, 571–576.
7. Song, J. H.; Atay, T.; Shi, S. F.; Urabe, H.; Nurmikko, A. V. Large Enhancement of Fluorescence Efficiency from CdSe/ZnS Quantum Dots Induced by Resonant Coupling to Spatially Controlled Surface Plasmons. *Nano Lett.* **2005**, *5*, 1557–1561.
8. Lunz, M.; Gerard, V. A.; Gun'ko, Y. K.; Lesnyak, V.; Gaponik, N.; Susha, A. S.; Rogach, A. L.; Bradley, A. L. Surface Plasmon Enhanced Energy Transfer between Donor and Acceptor CdTe Nanocrystal Quantum Dot Monolayers. *Nano Lett.* **2011**, *11*, 3341–3345.
9. Kulakovich, O.; Strekal, N.; Yaroshevich, A.; Maskevich, S.; Gaponenko, S.; Nabiev, I.; Woggon, U.; Artemyev, M. Enhanced Luminescence of CdSe Quantum Dots on Gold Colloids. *Nano Lett.* **2002**, *2*, 1449–1452.
10. Kuhn, S.; Hakanson, U.; Rogobete, L.; Sandoghdar, V. Enhancement of Single-Molecule Fluorescence Using a Gold Nanoparticle as an Optical Nanoantenna. *Phys. Rev. Lett.* **2006**, *97*, 017402.
11. Anger, P.; Bharadwaj, P.; Novotny, L. Enhancement and Quenching of Single-Molecule Fluorescence. *Phys. Rev. Lett.* **2006**, *96*, 113002.
12. Sun, G.; Khurgin, J. B.; Soref, R. A. Practical Enhancement of Photoluminescence by Metal Nanoparticles. *Appl. Phys. Lett.* **2009**, *94*, 101103.
13. Acuna, G. P.; Bucher, M.; Stein, I. H.; Steinhauer, C.; Kuzyk, A.; Holzmeister, P.; Schreiber, R.; Moroz, A.; Stefani, F. D.; Liedl, T.; et al. Distance Dependence of Single-Fluorophore Quenching by Gold Nanoparticles Studied on DNA Origami. *ACS Nano* **2012**, *6*, 3189–3195.
14. Reineck, P.; Gomez, D.; Ng, S. H.; Karg, M.; Bell, T.; Mulvaney, P.; Bach, U. Distance and Wavelength Dependent Quenching of Molecular Fluorescence by Au@SiO_2 Core−Shell Nanoparticles. *ACS Nano* **2013**, *7*, 6636–6648.
15. Barrow, S. J.; Wei, X.; Baldauf, J. S.; Funston, A. M.; Mulvaney, P. The Surface Plasmon Modes of Self-Assembled Gold Nanocrystals. *Nat. Commun.* **2012**, *3*, 1–9.
16. Yan, W.; Xu, L.; Xu, C.; Ma, W.; Kuang, H.; Wang, L.; Kotov, N. A. Self-Assembly of Chiral Nanoparticle Pyramids with Strong R/S Optical Activity. *J. Am. Chem. Soc.* **2012**, *134*, 15114–15121.
17. Govorov, A. O.; Fan, Z.; Hernandez, P.; Slocik, J. M.; Naik, R. R. Theory of Circular Dichroism of Nanomaterials Comprising Chiral Molecules and Nanocrystals: Plasmon Enhancement, Dipole Interactions, and Dielectric Effects. *Nano Lett.* **2010**, *10*, 1374–1382.
18. Kuzyk, A.; Schreiber, R.; Fan, Z.; Pardatscher, G.; Roller, E.-M.; Högele, A.; Simmel, F. C.; Govorov, A. O.; Liedl, T. DNA-Based Self-Assembly of Chiral Plasmonic Nanostructures with Tailored Optical Response. *Nature* **2012**, *483*, 311–314.
19. Mastroianni, A. J.; Claridge, S. A.; Alivisatos, A. P. Pyramidal and Chiral Groupings of Gold Nanocrystals Assembled Using DNA Scaffolds. *J. Am. Chem. Soc.* **2009**, *131*, 8455–8459.
20. Nykypanchuk, D.; Maye, M. M.; van der Lelie, D.; Gang, O. DNA-Guided Crystallization of Colloidal Nanoparticles. *Nature* **2008**, *451*, 549–552.
21. Park, S. Y.; Lytton-Jean, A. K. R.; Lee, B.; Weigand, S.; Schatz, G. C.; Mirkin, C. A. DNA-Programmable Nanoparticle Crystallization. *Nature* **2008**, *451*, 553–556.
22. Xu, P. F.; Lee, J. H.; Ma, K.; Choi, C.; Jin, S.; Wanga, J.; Cha, J. N. Enhanced Raman Signals from Switchable Nanoparticle Probes. *Chem. Commun.* **2013**, *49*, 8994–8996.
23. Pal, S.; Dutta, P.; Wang, H.; Deng, Z.; Zou, S.; Yan, H.; Liu, Y. Quantum Efficiency Modification of Organic Fluorophores Using Gold Nanoparticles on DNA Origami Scaffolds. *J. Phys. Chem. C* **2013**, *117*, 12735–12744.
24. Dutta, P. K.; Varghese, R.; Nangreave, J.; Lin, S.; Yan, H.; Liu, Y. DNA-Directed Artificial Light-Harvesting Antenna. *J. Am. Chem. Soc.* **2011**, *133*, 11985–11993.

25. Pilo-Pais, M.; Watson, A.; Demers, S.; LaBean, T. H.; Finkelstein, G. Surface-Enhanced Raman Scattering Plasmonic Enhancement Using DNA Origami-Based Complex Metallic Nanostructures. *Nano Lett.* **2014**, *14*, 2099–2104.
26. Xiong, H.; Sfeir, M. Y.; Gang, O. Assembly, Structure and Optical Response of Three-Dimensional Dynamically Tunable Multicomponent Superlattices. *Nano Lett.* **2010**, *10*, 4456–4462.
27. Young, K. L.; Ross, M. B.; Blaber, M. G.; Rycenga, M.; Jones, M. R.; Zhang, C.; Senesi, A. J.; Lee, B.; Schatz, G. C.; Mirkin, C. A. Using DNA To Design Plasmonic Metamaterials with Tunable Optical Properties. *Adv. Mater.* **2013**, *26*, 653–659.
28. Maye, M. M.; Nykypanchuk, D.; Cuisinier, M.; van der Lelie, D.; Gang, O. Stepwise Surface Encoding for High-Throughput Assembly of Nanoclusters. *Nat. Mater.* **2009**, *8*, 388–391.
29. Sun, D. Z.; Gang, O. Binary Heterogeneous Superlattices Assembled from Quantum Dots and Gold Nanoparticles with DNA. *J. Am. Chem. Soc.* **2011**, *133*, 5252–5254.
30. Seelig, J.; Leslie, K.; Renn, A.; Kuhn, S.; Jacobsen, V.; van de Corput, M.; Wyman, C.; Sandoghdar, V. Nanoparticle-Induced Fluorescence Lifetime Modification as Nanoscopic Ruler: Demonstration at the Single Molecule Level. *Nano Lett.* **2007**, *7*, 685–689.
31. Jennings, T. L.; Singh, M. P.; Strouse, G. F. Fluorescent Lifetime Quenching near d = 1.5 nm Gold Nanoparticles: Probing NSET Validity. *J. Am. Chem. Soc.* **2006**, *128*, 5462–5467.
32. Yun, C. S.; Javier, A.; Jennings, T.; Fisher, M.; Hira, S.; Peterson, S.; Hopkins, B.; Reich, N. O.; Strouse, G. F. Nanometal Surface Energy Transfer in Optical Rulers, Breaking the FRET Barrier. *J. Am. Chem. Soc.* **2005**, *127*, 3115–3119.
33. Hartling, T.; Reichenbach, P.; Eng, L. M. Near-Field Coupling of a Single Fluorescent Molecule and a Spherical Gold Nanoparticle. *Opt. Express* **2007**, *15*, 12806–12817.
34. Gersten, J.; Nitzan, A. Spectroscopic Properties of Molecules Interacting with Small Dielectric Particles. *J. Chem. Phys.* **1981**, 1139–1152.
35. Yu, W. W.; Wang, Y. A.; Peng, X. G. Formation and Stability of Size-, Shape-, and Structure-Controlled CdTe Nanocrystals: Ligand Effects on Monomers and Nanocrystals. *Chem. Mater.* **2003**, *15*, 4300–4308.
36. Zang, H. D.; Routh, P. K.; Alam, R.; Maye, M. M.; Cotlet, M. Core Size Dependent Hole Transfer from a Photoexcited CdSe/ZnS Quantum Dot to a Conductive Polymer. *Chem. Commun.* **2014**, *50*, 5958–5960.
37. Zhang, Y. G.; Lu, F.; Yager, K. G.; van der Lelie, D.; Gang, O. A General Strategy for the DNA-Mediated Self-Assembly of Functional Nanoparticles into Heterogeneous Systems. *Nat. Nanotechnol.* **2013**, *8*, 865–872.
38. Xiong, H. M.; van der Lelie, D.; Gang, O. Phase Behavior of Nanoparticles Assembled by DNA Linkers. *Phys. Rev. Lett.* **2009**, *102*, 015504.
39. Gueroui, Z.; Libchaber, A. Single-Molecule Measurements of Gold-Quenched Quantum Dots. *Phys. Rev. Lett.* **2004**, *93*, 166108.
40. Pons, T.; Medintz, I. L.; Sapsford, K. E.; Higashiya, S.; Grimes, A. F.; English, D. S.; Mattoussi, H. On the Quenching of Semiconductor Quantum Qot Photoluminescence by Proximal Gold Nanoparticles. *Nano Lett.* **2007**, *7*, 3157–3164.
41. Li, M.; Cushing, S. K.; Wang, Q. Y.; Shi, X. D.; Hornak, L. A.; Hong, Z. L.; Wu, N. Q. Size-Dependent Energy Transfer between CdSe/ZnS Quantum Dots and Gold Nanoparticles. *J. Phys. Chem. Lett.* **2011**, *2*, 2125–2129.
42. Stryer, L.; Haugland, R. P. Energy Transfer—A Spectroscopic Ruler. *Proc. Natl. Acad. Sci. U.S.A.* **1967**, *58*, 719–726.
43. Medintz, I. L.; Mattoussi, H. Quantum Dot-Based Resonance Energy Transfer and Its Growing Application in Biology. *Phys. Chem. Chem. Phys.* **2009**, *11*, 17–45.
44. Patra, D.; Gregor, I.; Enderlein, J.; Sauer, M. Defocused Imaging of Quantum-Dot Angular Distribution of Radiation. *Appl. Phys. Lett.* **2005**, *87*, 101103.
45. Bharadwaj, P.; Anger, P.; Novotny, L. Nanoplasmonic Enhancement of Single-Molecule Fluorescence. *Nanotechnology* **2007**, *18*, 044017.
46. Peng, B.; Li, Z. P.; Mutlugun, E.; Martinez, P. L. H.; Li, D. H.; Zhang, Q.; Gao, Y.; Demir, H. V.; Xiong, Q. H. Quantum Dots on Vertically Aligned Gold Nanorod Monolayer: Plasmon Enhanced Fluorescence. *Nanoscale* **2014**, *6*, 5592–5598.
47. Tam, F.; Goodrich, G. P.; Johnson, B. R.; Halas, N. J. Plasmonic Enhancement of Molecular Fluorescence. *Nano Lett.* **2007**, *7*, 496–501.
48. Sun, D. Z.; Gang, O. DNA-Functionalized Quantum Dots: Fabrication, Structural, and Physicochemical Properties. *Langmuir* **2013**, *29*, 7038–7046.